NASA
Technical Memorandum 88826

USAAVSCOM
Technical Report 86-C-26

Effect of Vibration Amplitude on Vapor Cavitation in Journal Bearings

David E. Brewe
Propulsion Directorate
U.S. Army Aviation Research and Technology Activity—AVSCOM
Lewis Research Center
Cleveland, Ohio

and

Bo O. Jacobson
University of Luleå
Luleå, Sweden

Prepared for the
Nordic Symposium on Tribology
sponsored by Royal Swedish Academy of Engineering Sciences
Luleå, Sweden, June 15–18, 1986

NASA

EFFECT OF VIBRATION AMPLITUDE ON VAPOR CAVITATION IN JOURNAL BEARINGS

David E. Brewe
Propulsion Directorate
U.S. Army Aviation Research and Technology Activity - AVSCOM
Lewis Research Center
Cleveland, Ohio 44135

and

Bo O. Jacobson
University of Luleå
Luleå, Sweden

SUMMARY

Computational movies were used to analyze the formation and collapse of vapor cavitation bubbles in a submerged journal bearing. The effect of vibration amplitude on vapor cavitation was studied for a journal undergoing circular whirl. The boundary conditions were implemented using Elrod's algorithm, which conserves mass flow through the cavitation bubble as well as through the oil-film region of the bearing. The vibration amplitudes for the different cases studied resulted in maximum eccentricity ratios ranging from 0.4 to 0.9. The minimum eccentricity ratio reached in each case was 0.1. For the least vibration amplitude studied in which the eccentricity ratio varied between 0.1 and 0.4, no vapor cavitation occurred. The largest vibration amplitude (i.e., eccentricity ratios of 0.1 to 0.9) resulted in vapor cavitation present 76 percent of one complete orbit.

INTRODUCTION

Vapor cavitation in submerged journal bearings is a type of cavitation that is only present when the bearing is in a dynamic state. Normally vapor cavitation appears during some part of a vibration when the dynamic loading on a bearing results in a rapid increase of the minimum oil-film thickness. Surface separation due to normal motion causes film pressure to decrease until the tensile strength of the oil or the bonding strength of the oil to the bearing surfaces is exceeded. The cavitation bubble produced contains mostly oil vapor of a very low pressure (close to vacuum).

Quite frequently, vapor cavitation produces erosion on the bearing surfaces when the vapor bubbles are transported to a high-pressure area of the lubricating film where they collapse. The presence of vapor cavitation also changes the dynamic behavior of the bearing. In particular, the damping in the bearing decreases considerably.

The phenomenon of vapor cavitation in journal bearings was experimentally studied by Jacobson and Hamrock (refs. 1 and 2). They found that the size of the vapor cavitation zone was dependent on factors such as the vibration amplitude, the minimum oil-film thickness reached during a vibration, and the surface energy of the bearing surfaces.

This report is a theoretical-numerical investigation of the appearance, growth, collapse, and disappearance of the vapor cavitation zone for a submerged journal bearing. A computer program was developed (ref. 3) which uses Elrod's algorithm for the continuity of mass flow into, through, and out of the vapor cavitation zone. This program makes it possible to predict the dynamic behavior of the vapor cavitation zone. The Cray computer at NASA Lewis Research Center was used to do the computations.

SYMBOLS

D	shaft diameter, m
e	eccentricity
g	switch function (cavitation index)
h	film thickness, m
L	bearing length, m
L/D	length to diameter ratio
$\vec{\dot{m}}$	lineal mass flux, kg/m-s
P	fluid pressure, N/m^2
P_a	ambient fluid pressure, N/m^2
P_c	cavitation fluid pressure, N/m^2
R	radius of shaft, m
ΔR	radial clearance, m
t	time, s
U	sum of surface velocities in x-direction, m/s
$\vec{V}$	sum of surface velocity vectors, m/s
W	load capacity, N
w	squeeze-velocity, m/s
x	coordinate along circumference, m
y	coordinate normal to x,z plane, m
z	axial coordinate, m
β	liquid bulk modulus, N/m^2
γ	angular position of minimum film, rad
ε	eccentricity ratio, $e/\Delta R$

θ fractional film content in cavitation zone; density ratio (ρ/ρ_c) in full-film zone

μ dynamic viscosity, N-s/m^2

ρ fluid density within full-film zone, kg/m^3

ρ_c fluid density within cavitated zone, kg/m^3

φ angular coordinate relative to minimum film line, rad

ω_d orbital angular velocity of journal center about fixed point relative to housing center, rad/s

ω_s angular velocity of journal about its own center, rad/s

Subscripts:

max maximum

min minimum

BACKGROUND THEORY

Elrod and Adams (ref. 4), implemented a moving boundary scheme that avoids interface complications. The following is a review of some of the underlying factors that led to the algorithm which was later modified by Elrod (ref. 5) and used here. The conservation of mass can be written as

$$\frac{\partial(\rho h)}{\partial t} + \vec{\nabla} \cdot \left(\dot{\vec{m}} \right) = 0 \tag{1}$$

where $\dot{\vec{m}}$ represents the lineal mass flux and is given by

$$\dot{\vec{m}} = \rho \frac{h\vec{V}}{2} - \frac{\rho h^3}{12\mu} \vec{\nabla} P \tag{2}$$

Substituting equation (2) into equation (1) yields the Reynolds lubrication equation. This equation is made applicable to the cavitation region as well as to the full-film region by incorporating a switching function that automatically satisfies the boundary conditions at a moving interface. Furthermore, the fractional film content θ is made the dependent variable. This requires giving θ a dual interpretation. That is, in the full-film region, θ represents the mass content of the film that exceeds the content at the cavitation pressure P_c. In other words,

$$\theta = \frac{\rho}{\rho_c} \tag{3}$$

where ρ_c is the density of the liquid at P_c. Furthermore, P and ρ are related through the equation for the liquid bulk modulus according to

$$\rho \frac{\partial P}{\partial \rho} = \beta \tag{4}$$

or

$$P = P_c + \beta \ln \theta \qquad \theta \geq 1.0 \tag{5}$$

In the cavitation region $\theta \leq 1.0$, θ determines the mass content $\rho_c \theta h$, which can manifest itself in the form of a smeared mass or striated flow extending to both surfaces in the film gap. The fluid transported through the cavitation region in the form of an adhered film can be neglected for heavily loaded conditions.

A universal differential equation is made possible by linking the solutions of the full-film region with the solutions in the cavitated region by a single dependent variable θ. However, a cavitation index, or switch function g, was included so that the resulting partial differential equation would be consistent with the uniform pressure assumption within the cavitated region. The switch function is defined from a knowledge of θ. Thus,

$$\left.\begin{aligned} g &= 0 \qquad \theta \leq 1.0 \\ g &= 1 \qquad \theta > 1.0 \end{aligned}\right\} \tag{6}$$

The switch function g is made a factor of the pressure gradient term in equation (2) so that the flow is strictly Couette in the cavitated region. Expressing the lineal mass flux $\dot{\vec{m}}$ in terms of θ and g and substituting it into equation 1 yield the universal differential equation obtained by Elrod and Adams (ref. 4):

$$\frac{\partial(\theta h)}{\partial t} + \frac{\vec{V}}{2} \cdot \left[\vec{\nabla}(\theta h)\right] = \vec{\nabla} \cdot \left[\frac{h^3}{12\mu} \beta g(\theta) \vec{\nabla}\theta\right] \tag{7}$$

In the full-film region the solutions of θ together with equation (5) determine the pressures. In the cavitation region, $g = 0$ and equation (7) becomes

$$\frac{\partial(\theta h)}{\partial t} + \frac{\vec{V}}{2} \cdot \left[\vec{\nabla}(\theta h)\right] = 0 \tag{8}$$

Equation (8) governs the transport of the fluid through the cavitation region.

The numerical details are given in Brewe's work (ref. 3) as well as in the original publications by Elrod and Adams (ref.4) and Elrod (ref. 5). The method combines a control volume approach to deriving the finite-difference equations with the use of a switching function to automatically satisfy the boundary conditions at a moving interface. An alternating direction implicit scheme is applied. At each half-time step the implicit Euler method is used to march in time. This method is known to be unconditionally stable (ref. 6) insofar as the ordinary differential equation is stable. In the first half-time step, spacial differencing along the circumferential direction results in a periodic tridiagonal matrix. The solutions for θ and, consequently, ρ are found by performing a Gauss-Jordan reduction on the matrix along with a maximum-pivot strategy to reduce the error. Spacial differencing along the axial direction is performed to complete the time step. The solutions for this sweep are more readily obtained by using a nonpivoted Gaussian elimination procedure (tri-

diagonal solver). Since the journal and housing are aligned, the pressures must be symmetric about the axial center. Consequently, the calculations are only made over half the axial length of the housing.

RESULTS AND DISCUSSION

Cavitation and Pressure Distribution

The effect of vibration amplitude on vapor cavitation was studied for a journal undergoing circular whirl. The journal bearing configuration is shown in figure 1. The range of amplitudes and conditions considered in this study are listed in table I.

Figures 2 to 4 illustrate the pressure history within the fluid-film region for a journal completing one orbit of its cycle. Figure 2 represents the case in which $0.1 \leq \varepsilon \leq 0.9$. The maximum vibration amplitudes in figures 3 and 4 resulted in ε_{max} of 0.7 and 0.5, respectively. As the maximum vibration amplitude is decreased (i.e., $\varepsilon_{max} = 0.9$, 0.7, and 0.5) the size and life of the bubble decrease (i.e., t = 49.4 ms, 42.1 ms, and 20.5 ms) respectively. For $\varepsilon_{max} = 0.4$, cavitation was not present.

Figure 2(a) represents the position of the journal within the housing and the associated pressure distribution at the instant that the eccentricity is a minimum. The dark oblong region indicates the shape and position of a vapor bubble downstream of the minimum-film line. The position of the bubble within the small clearance space of the journal bearing is also indicated. At this particular instant the tendency of the pressure flow along the side of the bubble to cause the bubble to collapse is becoming greater since it is proportional to h^3. The journal center moves in a clockwise orbit from figure 2(a) to (b) (nearly one-quarter of a revolution). While the eccentricity is increasing, the minimum film is decreasing - giving rise to the squeeze action in the vicinity of the minimum-film line. A slight rise in the pressure field can be observed there. Note however that the vapor bubble has moved further downstream from its position in 2(a). It is now located at the position of maximum film thickness. The increased side flow will cause total bubble collapse.

From figure 2(b) to (c) cavitation is absent. In figure 2(c), a new cavitation bubble appears and the pressure generation in the region of the minimum-film line becomes significantly large because of the squeeze and wedge effect taking place there. Figure 2(d) represents the configuration of the bearing when the maximum pressure occurs. Note that this happens 3.5 ms before the maximum eccentricity is reached because of the motion of the shaft (fig. 5). As the journal approaches the end of the squeeze cycle and begins to separate from the shaft, the sliding velocity approaches a minimum value and the squeeze velocity passes through zero. The effect this has on the pressures more than offsets any increase in pressure that would have been realized because of the smaller minimum film thickness.

Figure 2(e) represents the end of the squeeze cycle illustrating this reverse effect. Now the minimum film thickness begins to increase, creating a suction effect, an accompanying growth in the bubble, and a complete dissipation of the pressure hump noted in 2(f). It is interesting to note that the

eccentricity is the same (0.83) for figures 2(c) and (f). The drastic difference in the pressure plot is a result of the squeeze velocity having opposite signs in the two situations. The minimum film thickness continues to increase as it moves in a clockwise direction. The representation shown in figure 2(a) is repeated as is each of the representations for each succeeding orbit.

Load Capacity Versus Eccentricity

Figures 6(a) to (d) represent the load capacity as a function of eccentricity for different vibration amplitudes. The predominant effect to note in these figures is that the cavitation produces a hysteresis effect in the load cycle. As previously noted, the size and life of the bubble decrease with decreasing vibration amplitude. The hysteresis effect is more pronounced for higher vibration amplitudes. In figure 6(d) the maximum eccentricity reached in the load cycle was 0.4 and cavitation was absent. The absence of cavitation resulted in a load cycle without hysteresis.

CONCLUSIONS

The following conclusions can be stated for those cases in which the vibration amplitude is increasing:

1. The vapor bubble life increases.

2. Maximum vapor bubble size increases.

3. The bubble inception comes earlier and the bubble collapse comes later.

4. The variation of the load-carrying capacity increases.

5. The load cycle changes from nonhysteretic to hysteretic when vapor cavitation occurs.

REFERENCES

1. Jacobson, B.O.; and Hamrock, B.J.: High-Speed Motion Picture Camera Experiments of Cavitation in Dynamically Loaded Journal Bearings. J. Lubr. Technol., vol. 105, no. 3, July 1983, pp. 446-452.

2. Jacobson, B.O.; and Hamrock, B.J.: Vapor Cavitation in Dynamically Loaded Journal Bearings. Second International Conference on Cavitation, Inst. Mech. Eng., 1983, pp. 133-140.

3. Brewe, D.E.: Theoretical Modeling of the Vapor Cavitation in Dynamically Loaded Journal Bearings. NASA TM-87076, 1985.

4. Elrod, H.G.; and Adams, M.L.: A Computer Program for Cavitation and Starvation Problems. Cavitation and Related Phenomena in Lubrication, D. Dowson, M. Godet, and C.M. Taylor, eds., Mechanical Engineering Publications, Ltd., 1975, pp. 37-41.

5. Elrod, H.G.: A Cavitation Algorithm. J. Lubr. Technol., vol. 103, no. 3, July 1981, pp. 350-354.

6. Warming, R.F.; and Beam, R.M.: An Extension of A-Stability to Alternating Direction Implicit Methods. NASA TM-78537, 1978.

TABLE I. - OPERATING CONDITIONS

Radial clearance, ΔR, mm	0.5
Radius of shaft, R, mm	42.5
Length to diameter ratio	1.0
Eccentricity ratio, ε	0.1 to ε_{max}
Maximum eccentricity ratio, ε_{max}	0.4 to 0.9
Angular velocity of journal about its own center, ω_s, rad/s	-19.5
Orbital angular velocity of journal center about fixed point relative to housing center, ωd, rad/s	-92.7
Liquid bulk modulus, β, N/m^2	1.72×10^9
Dynamic viscosity, μ, $N\text{-}s/m^2$	0.066
Ambient pressure, P_a, N/m^2	1.0133×10^5
Cavitation pressure, P_c, N/m^2	0.0

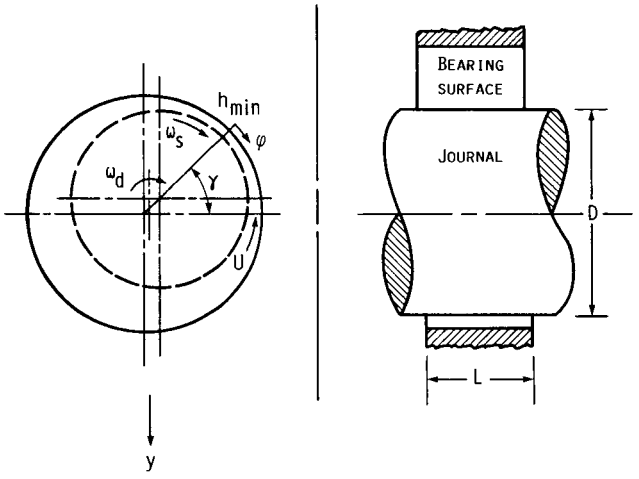

FIGURE 1.- JOURNAL BEARING CONFIGURATION.

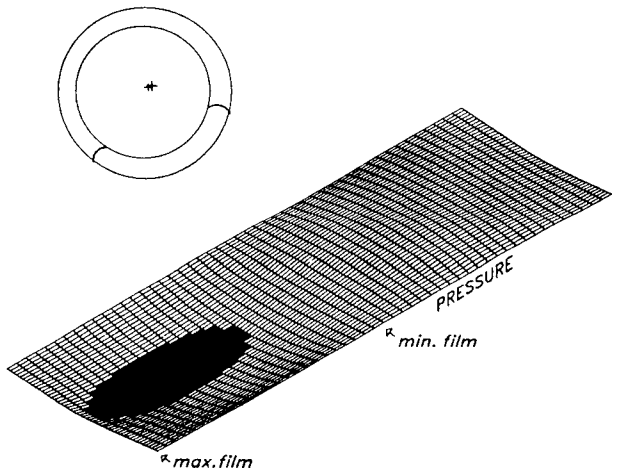

(A) ROTOR AT MAXIMUM SEPARATION ($t = 0$; $\varepsilon = 0.10$).

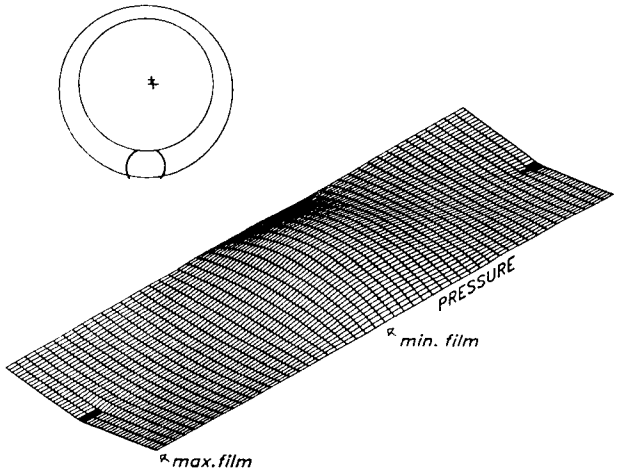

(B) BUBBLE COLLAPSE ($t = 7.03$ ms; $\varepsilon = 0.30$).

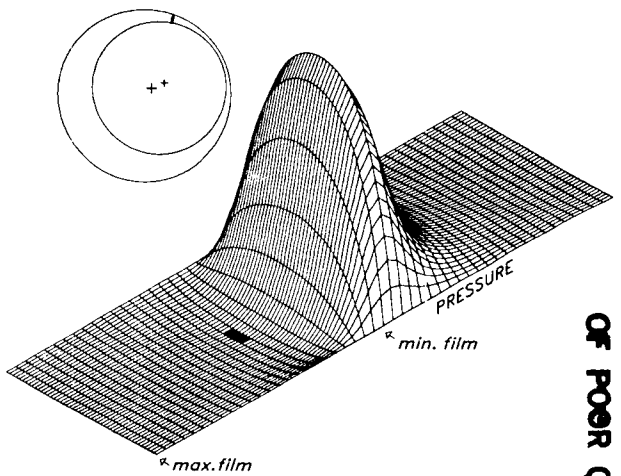

(C) CAVITATION INCEPTION ($t = 25.41$ ms; $\varepsilon = 0.83$).

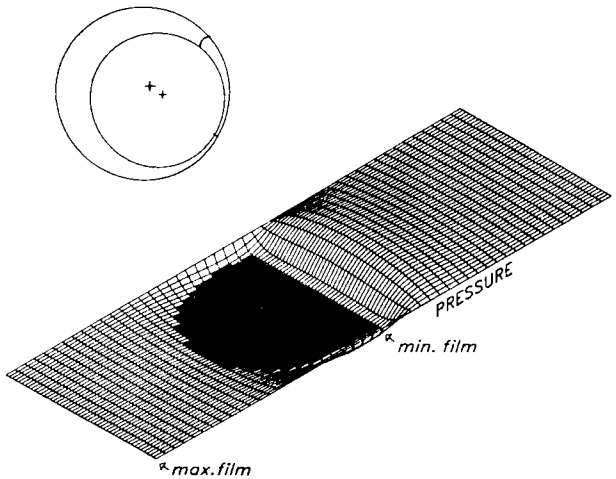

(F) BUBBLE EXPANDS ($t = 42.51$ ms; $\varepsilon = 0.83$).

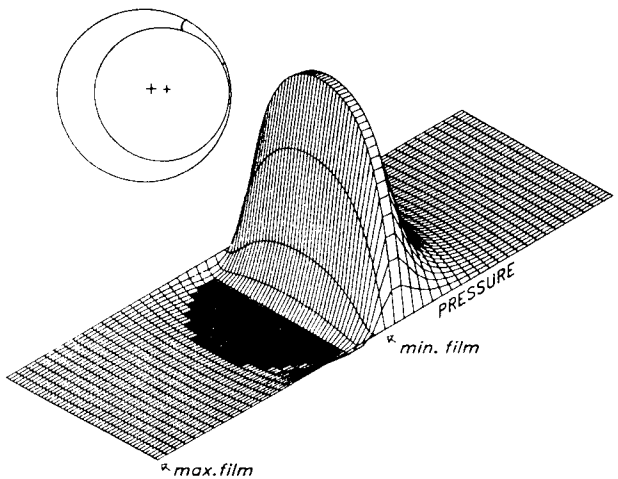

(E) BEGIN SEPARATION ($t = 33.89$ ms; $\varepsilon = 0.90$).

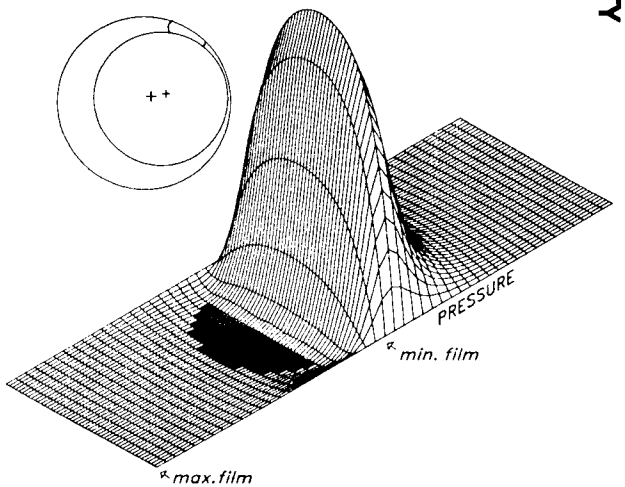

(D) OCCURRENCE OF PEAK PRESSURE ($t = 29.31$ ms; $\varepsilon = 0.88$).

FIGURE 2.- PRESSURE DISTRIBUTION AND BEARING CONFIGURATION FOR A FULL PERIOD OF SHAFT WHIRL, ($0.1 \leq \varepsilon \leq 0.9$). (FIGURES (A) TO (F) VIEWED CLOCKWISE ARE CONSECUTIVE IN TIME.)

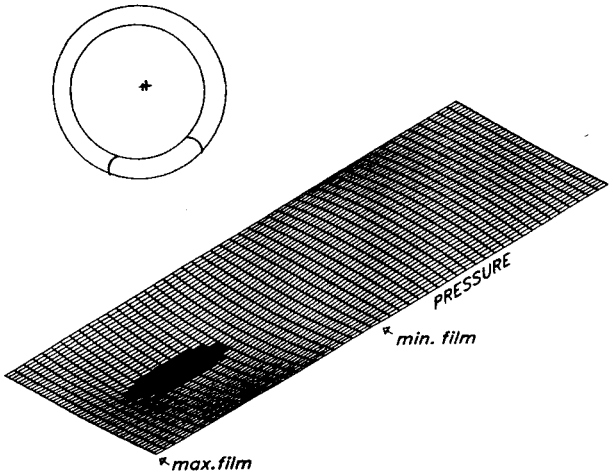

(A) ROTOR AT MAXIMUM SEPARATION ($t = 0$; $\varepsilon = 0.10$).

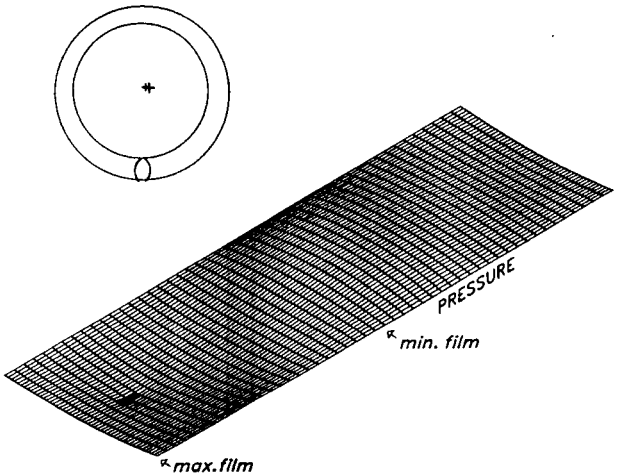

(B) BUBBLE COLLAPSE ($t = 3.03$ ms; $\varepsilon = 0.14$).

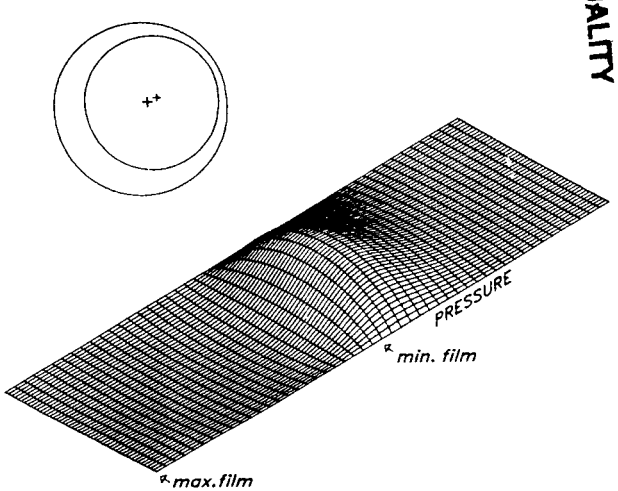

(C) OCCURRENCE OF PEAK PRESSURE ($t = 25.11$ ms; $\varepsilon = 0.64$).

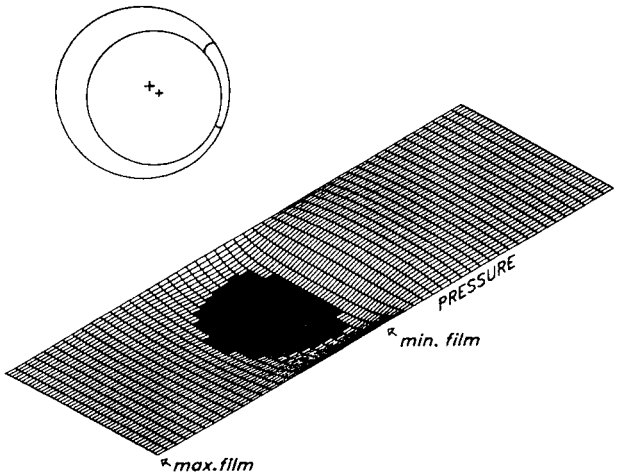

(F) BUBBLE EXPANDS ($t = 42.71$ ms; $\varepsilon = 0.70$).

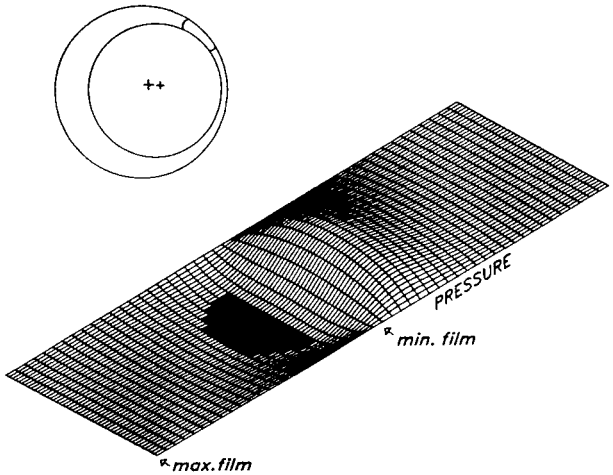

(E) BEGIN SEPARATION ($t = 33.89$ ms; $\varepsilon = 0.70$).

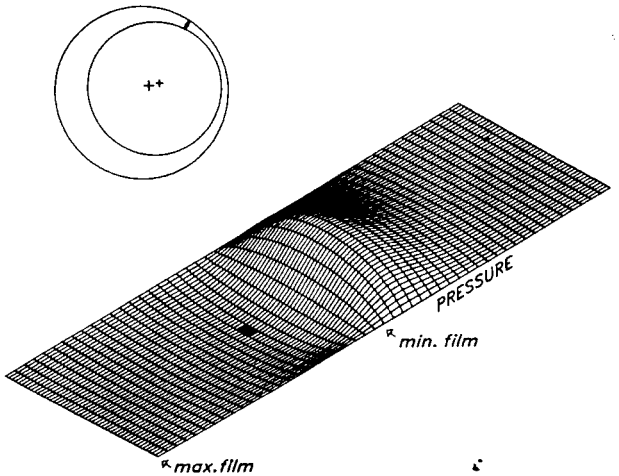

(D) CAVITATION INCEPTION ($t = 28.71$ ms; $\varepsilon = 0.68$).

FIGURE 3.- PRESSURE DISTRIBUTION AND BEARING CONFIGURATION FOR A FULL PERIOD OF SHAFT WHIRL, ($0.1 \leq \varepsilon \leq 0.7$). FIGURES (A) TO (F) VIEWED CLOCKWISE ARE CONSECUTIVE IN TIME.

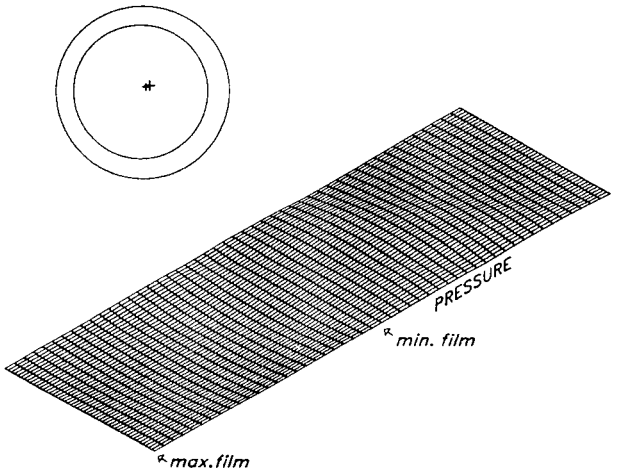

(A) ROTOR AT MAXIMUM SEPARATION (t = 0; ε =0.10).

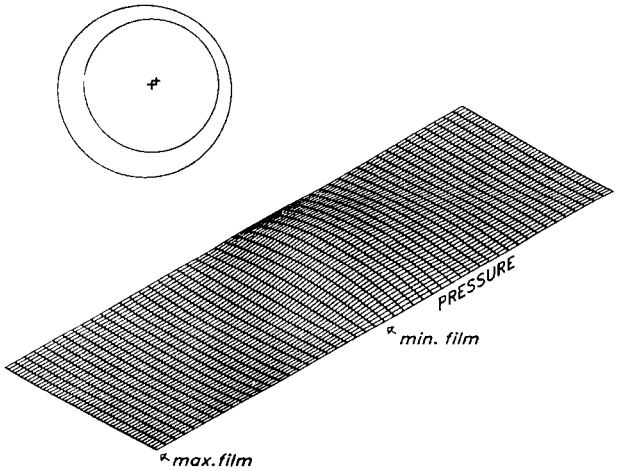

(B) OCCURRENCE OF PEAK PRESSURE (t = 21.90 ms; ε = 0.43).

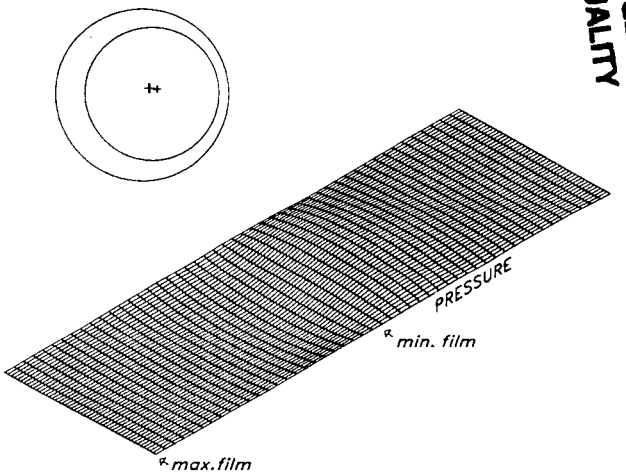

(C) BEGIN SEPARATION (t = 33.89 ms; ε = 0.5).

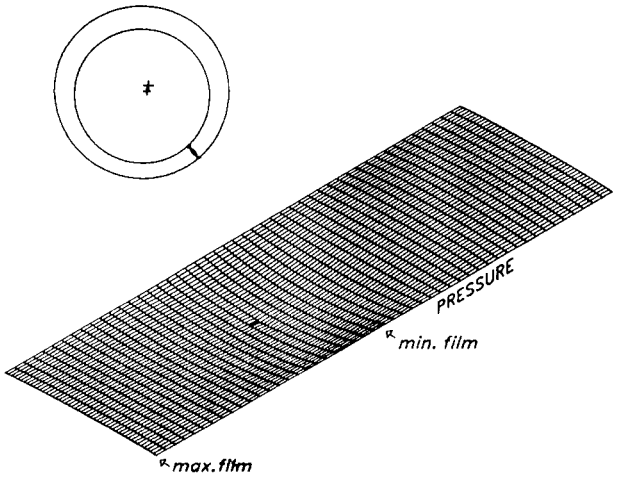

(F) BUBBLE COLLAPSE (t = 58.61 ms; ε = 0.23).

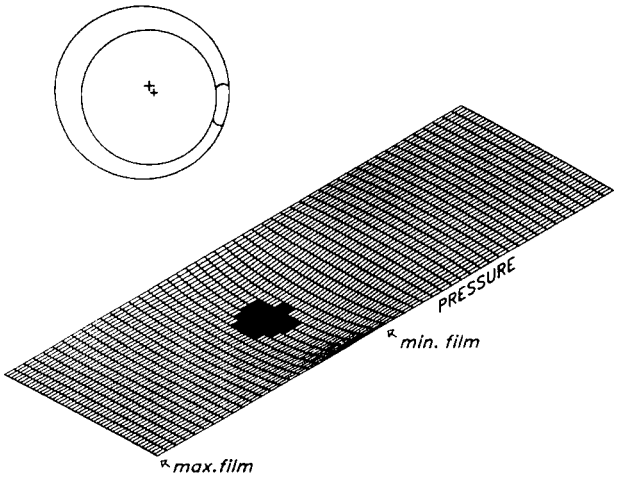

(E) BUBBLE EXPANDS (t = 45.91 ms; ε = 0.43).

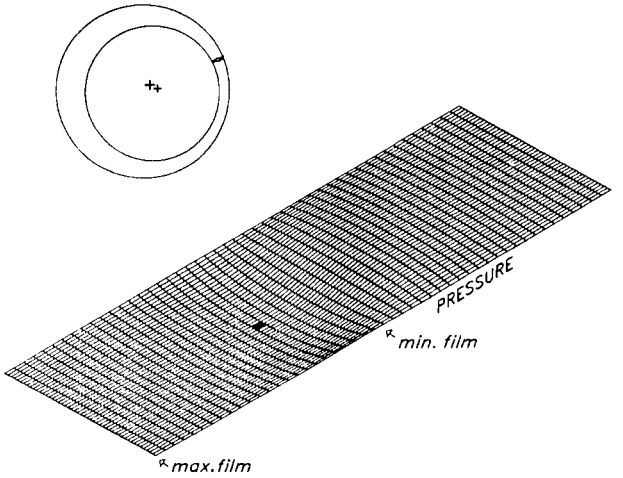

(D) CAVITATION INCEPTION (t = 37.91 ms; ε = 0.49).

FIGURE 4.- PRESSURE DISTRIBUTION AND BEARING CONFIGURATION FOR A FULL PERIOD OF SHAFT WHIRL ($0.1 \leq \varepsilon \leq 0.5$). (FIGURES (A) TO (F) VIEWED CLOCKWISE ARE CONSECUTIVE IN TIME.)

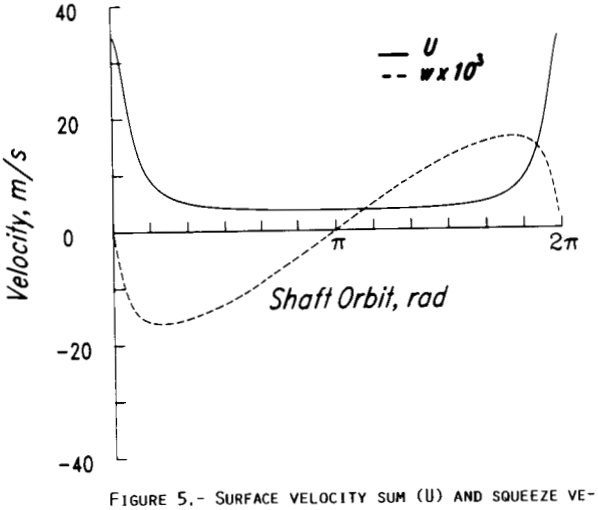

FIGURE 5.- SURFACE VELOCITY SUM (U) AND SQUEEZE VELOCITY (W) DURING A FULL PERIOD OF SHAFT WHIRL.

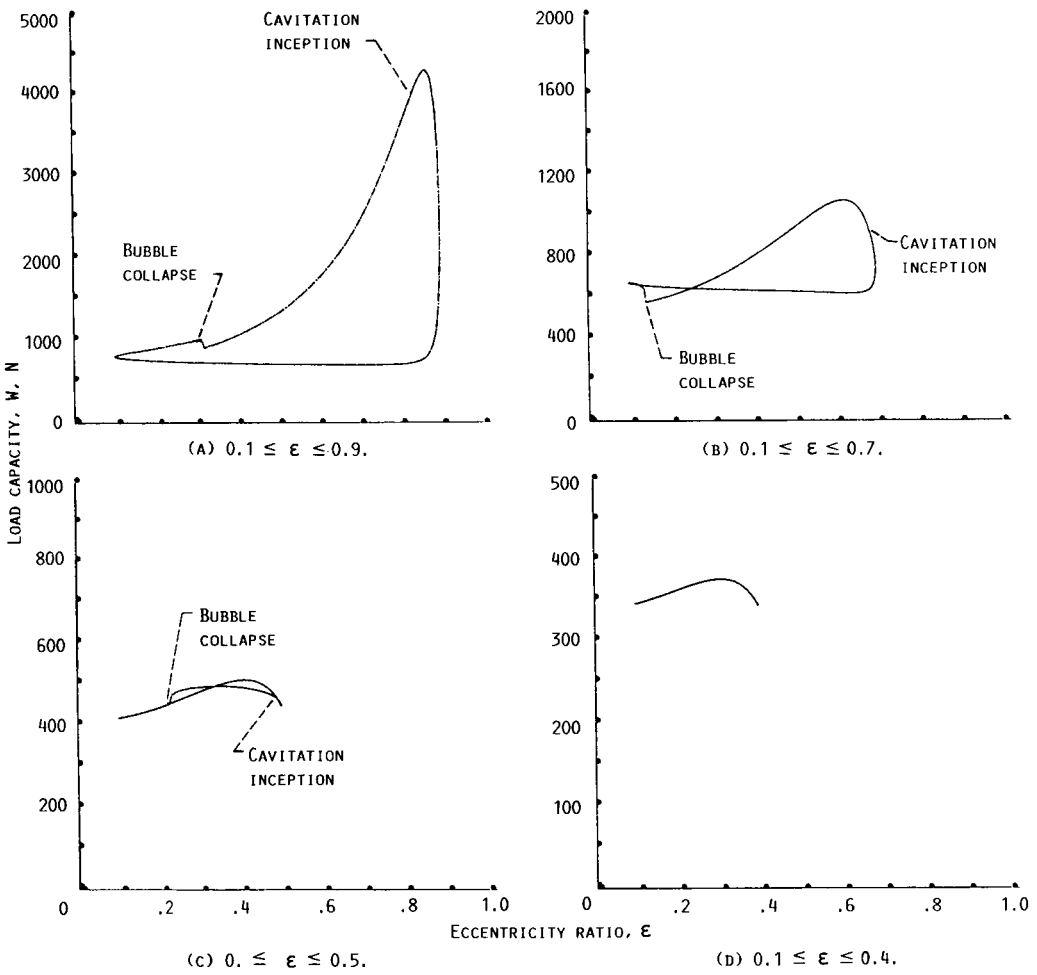

(A) $0.1 \leq \varepsilon \leq 0.9$.

(B) $0.1 \leq \varepsilon \leq 0.7$.

(C) $0. \leq \varepsilon \leq 0.5$.

(D) $0.1 \leq \varepsilon \leq 0.4$.

FIGURE 6.- LOAD CAPACITY AS FUNCTION OF ECCENTRICITY RATIO FOR FOUR VIBRATION AMPLITUDES.

1. Report No. NASA TM-88826 USAAVSCOM-TR-86-C-26	2. Government Accession No.	3. Recipient's Catalog No.

4. Title and Subtitle	5. Report Date
Effect of Vibration Amplitude on Vapor Cavitation in Journal Bearings	6. Performing Organization Code 505-63-81
7. Author(s) David E. Brewe and Bo O. Jacobson	8. Performing Organization Report No. E-3200
	10. Work Unit No.
9. Performing Organization Name and Address NASA Lewis Research Center and Propulsion Directorate, U.S. Army Aviation Research and Technology Activity - AVSCOM, Cleveland, Ohio 44135	11. Contract or Grant No.
	13. Type of Report and Period Covered Technical Memorandum
12. Sponsoring Agency Name and Address National Aeronautics and Space Administration Washington, D.C. 20546 and U.S. Army Aviation Systems Command, St. Louis, MO 63120	14. Sponsoring Agency Code

15. Supplementary Notes

Prepared for the Nordic Symposium on Tribology, sponsored by the Royal Swedish Academy of Engineering Sciences, Luleå, Sweden, June 15-18, 1986. David E. Brewe, Propulsion Directorate, U.S. Army Aviation Research and Technology - AVSCOM; Bo O. Jacobson, University of Luleå, Luleå, Sweden.

16. Abstract

Computational movies were used to analyze the formation and collapse of vapor cavitation bubbles in a submerged journal bearing. The effect of vibration amplitude on vapor cavitation was studied for a journal undergoing circular whirl. The boundary conditions were implemented using Elrod's algorithm, which conserves mass flow through the cavitation bubble as well as through the oil-film region of the bearing. The vibration amplitudes for the different cases studied resulted in maximum eccentricity ratios ranging from 0.4 to 0.9. The minimum eccentricity ratio reached in each case was 0.1. For the least vibration amplitude studied in which the eccentricity ratio varied between 0.1 and 0.4, no vapor cavitation occurred. The largest vibration amplitude (i.e., eccentricity ratios of 0.1 to 0.9) resulted in vapor cavitation present 76 percent of one complete orbit.

17. Key Words (Suggested by Author(s))	18. Distribution Statement
Journal bearings; Cavitation; Hydrodynamic; Dynamic loads; Circular whirl; Vibration; Vapor cavitation	Unclassified - unlimited STAR Category 34

19. Security Classif. (of this report)	20. Security Classif. (of this page)	21. No. of pages	22. Price*
Unclassified	Unclassified		

*For sale by the National Technical Information Service, Springfield, Virginia 22161